HiSST: 3rd International Conference on
High-Speed Vehicle Science Technology
14 -19 April 2024, Busan, Korea

Force Measurement in Shock Tunnel Tests Based on Deep Learning

Shaojun NIE[1], Yunpeng WANG[2]

Abstract

The aerodynamic force measurement conducted within shock tunnels bear paramount technological significance in the field of high-temperature aerodynamics. When a force test is conducted in a shock tunnel, vibration of the Force Measurement System (FMS) is excited under the strong flow impact, and it cannot be attenuated rapidly within the extremely short test duration of milliseconds order. The output signal of the force balance is coupled with the aerodynamic force and the inertial vibration. This interference can result in inaccurate force measurements, which can negatively impact the accuracy of the test results. To eliminate inertial vibration interference from the output signal, proposed here is a dynamic calibration modelling method for a FMS based on deep learning. The signal is processed using an intelligent Recurrent Neural Network (RNN) model in the time domain and an intelligent Convolutional Neural Network (CNN) model in the frequency domain. Results processed with the intelligent models show that the inertial vibration characteristics of the FMS can be identified efficiently. After processed by the intelligent models, high-precision aerodynamic force signals are obtained. Furthermore, the intelligent model method is applied to force measurement with the cone calibration model in shock tunnels. When compared with results from the force measurement database for the cone model, the relative deviation is less than 2%, validating the feasibility of applying deep learning methods in pulse-type shock tunnel balance force tests. The deep integration of deep learning with pulse tunnel force tests is of paramount significance in enhancing performance metrics for hypersonic aerodynamics tests. This exploratory research will also further propel the intelligent development of force measurement in shock tunnels.

Keywords: *Force Measurement, Shock Tunnel, Deep Learning, Intelligent Model*

Nomenclature

x – Original data
x* – Normalized data
RSD – Relative standard error
RD – Relative error
F – Value of the true force
F* - Value of the approximate force
A – Value of the reference load coefficient
A* - Value of the processed coefficient by AI model

Greek
δ – relative error

1. Introduction

To reduce the risk and cost of developing a new hypersonic vehicle, it is necessary to conduct ground tests in a high-enthalpy shock tunnel to test its aerodynamic performance. [1-3] As one of the most basic and important techniques in shock-tunnel tests, force measurement is an important way to obtain the aerodynamic data of an aircraft, and its measurement accuracy will directly affect the evaluation of aerodynamic characteristics. [4]

Measuring accurately the aerodynamic forces acting on a hypersonic vehicle in a millisecond shock

[1] *Affiliation: State Key Laboratory of High Temperature Gas Dynamics, Institute of Mechanics, Chinese Academy of Sciences, Address: No.15 Beisihuanxi Road, Beijing, China(100190), E-mail: nieshaojun@imech.ac.cn*
[2] *Affiliation: State Key Laboratory of High Temperature Gas Dynamics, Institute of Mechanics, Chinese Academy of Sciences, Address: No.15 Beisihuanxi Road, Beijing, China(100190), E-mail: wangyunpeng@imech.ac.cn*

tunnel still involves many key technical problems, the main one being the inertial vibration of the Force Measurement System (FMS), the main elements of which are the model, the wind-tunnel balance, and the supporting structure. [5-7] When a force test is carried out in a shock tunnel, disturbance of the complex flow field induces the inertial vibration with low frequency and high amplitude of the FMS, and the balance signal is mixed with the inertial vibration signals of the FMS, which makes it difficult to distinguish the dynamic characteristics of the aerodynamic signals directly and accurately. Therefore, it is very important to find a method to develop highly accurate force measurement technology for developing hypersonic vehicles.

To eliminate inertial vibration interference from balance output signals, much research has been conducted and various special balance technologies have been proposed. Currently, there are three main methods for improving force measurement technology, the first involving the development of the new FMS, examples include the stress-wave balance, [8-12] the piezoelectric balance, [13] the magnetic suspension balance, [14, 15] the free flight technique, [16-19] and the pulse-type strain-gauge balance. [20-22] However, there is a bottleneck to eliminate the influence of inertial vibration through developing a new FMS. The second method is to eliminate the influence of inertial vibration on the aerodynamic forces through signal compensation, examples being the accelerometer balance [23-26] and the inertial self-compensation balance. [27-29] The third method involves balance signal processing, such as wave system fitting, [30, 31] time-frequency transform, [32] Single-Vector Dynamic self-Calibration (SVDC), [33] and the intelligent identification algorithm, [34].

In summary, it is very difficult to improve the measurement accuracy by either improving the balance structure or using signal compensation. Instead, the deep cross application of AI in force tests has become a trend that has considerable engineering significance.

Fig 1 shows the part system of the JF-12 hypersonic detonation-driven shock tunnel with long test duration (referred to herein as the JF-12 shock tunnel).[35] The aim in this paper is to take the balance step signal as the input data and the ideal step signal as the target data and build an RNN time-domain model and a CNN frequency-domain model to learn the interference features; the intelligent models can identify and eliminate the interference signal and output a "pure" aerodynamic signal. The trained models are then ap-plied to a shock-tunnel force test to obtain aerodynamic signals without initial interference, thereby ensuring the accuracy of the force measurement results.

Fig 1. Partial photo of JF-12 shock tunnel

2. AI-based balance samples acquisition

2.1. Acquisition of balance samples in time domain

To ensure accuracy in a force test, it is necessary to perform dynamic calibration of the balance before the test. The traditional dynamic signal generation methods are impulse response [36,37] and step response. [38] These methods have strict requirements for the load direction, so they cannot be used for the dynamic calibration of a shock-tunnel balance. To meet the requirement that the balance outputs multicomponent load signals in any direction, the SVDC technology was proposed. [39] This method introduces deep-learning technology that can conduct modeling and processing for dynamic calibration in any direction and accurately identify the aerodynamic force coupled with inertial vibration interference.

Considering the operating factors of the JF-12 shock tunnel, the same step-load acquisition device based on SVDC was built outside the shock tunnel, comprising the model, the balance, and the supporting structure. As shown in Fig 2, the model was a standard cone with a length of 0.75 m and a half-cone angle of 10°, the balance was a three-component pulse-type strain-gauge balance, and the three components were the normal force, the pitching moment, and the axial force; the model and balance were supported by a cantilever sting.

FMS (model, balance and support)

Fig 2. Force Measurement System (FMS).

In this paper, dynamic calibration of the whole FMS was conducted based on SVDC technology. We collected 120 groups of the balance signal sample, and each sample comprised two groups of data: the balance step signal and the ideal step signal (corresponding to the input and target data, respectively, in the intelligent model). We selected a sample and plotted its waveform in the time domain, as shown in Fig 3, where the red line corresponds to the balance step signal (used to simulate the impact generated by the shock-tunnel flow field) and the blue line corresponds to the ideal step signal (used to simulate the simplified aerodynamic force signal). The sampling rate was 50 kHz and the total time for a sample was 150 ms, so the number of points per sample was 7500. The signal was divided into two sections by the starting moment of the flow field during the force test; the zero signal before the step corresponds to the preparation duration before the flow field started. At approximately 55 ms, the signal has a step change, and the edge trigger time can be ignored. Subsequently, the balance step signal contains both aerodynamic force and inertial vibration, whereas the ideal step signal contains no vibration signal and remains stable.

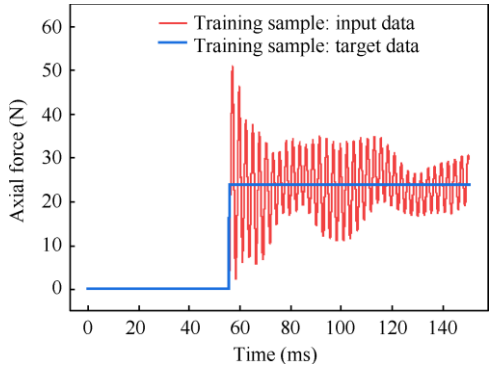

Fig 3. Balance sample waveform in time domain (axial force).

2.2. Time-frequency conversion of balance samples

The balance output signal collected during a force test is a typical unsteady and multifrequency impulse signal, and its waveform in the time domain reflects the aerodynamic trend directly. The frequency distribution of the signal can be displayed in the spectrum diagram in the frequency domain, and the vibration interference component can be distinguished by analyzing that diagram.

As a common signal processing method, a Fourier transform can decompose a signal linearly from the time domain into the frequency domain via the triangular basis function; similarly, an inverse Fourier transform can map a signal linearly from the frequency domain into the time domain. The respective transformation equations are

$$F(\omega) = \int_{-\infty}^{+\infty} f(t) e^{-i\omega t} dt \tag{1}$$

$$f(t)=\frac{1}{2\pi}\int_{-\infty}^{+\infty}F(\omega)e^{i\omega t}d\omega \tag{2}$$

where ω is frequency, $F(\omega)$ is the image function of $f(t)$, and $f(t)$ is the primitive function of $F(\omega)$.A Fast Fourier Transform (FFT) is used to convert the time-domain signal in Fig 3 into the frequency domain, and its spectrum diagram is shown in Fig 4. As can be seen, the main frequency of the balance step signal is approximately 380 Hz, whereas this frequency is absent from the ideal step signal, thereby indicating that the inertial vibration frequency of the FMS is approximately 380 Hz.

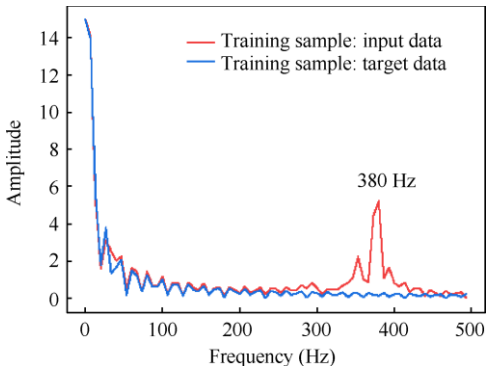

Fig 4. Balance sample spectrum diagram in frequency domain.

Because the time-domain signal offers a more direct reflection of the force trend, after analyzing the frequency-domain signal, the latter is transformed into the time domain using an Inverse FFT (IFFT). There may be some loss in the time-frequency conversion, but comparing the original balance signal with the signal after time-frequency conversion as shown in Fig 5, we can see that they basically coincide completely. This indicates that the loss in time-frequency conversion can be ignored completely, thereby providing a theoretical basis for the feasibility and reliability of data processing in the frequency domain.

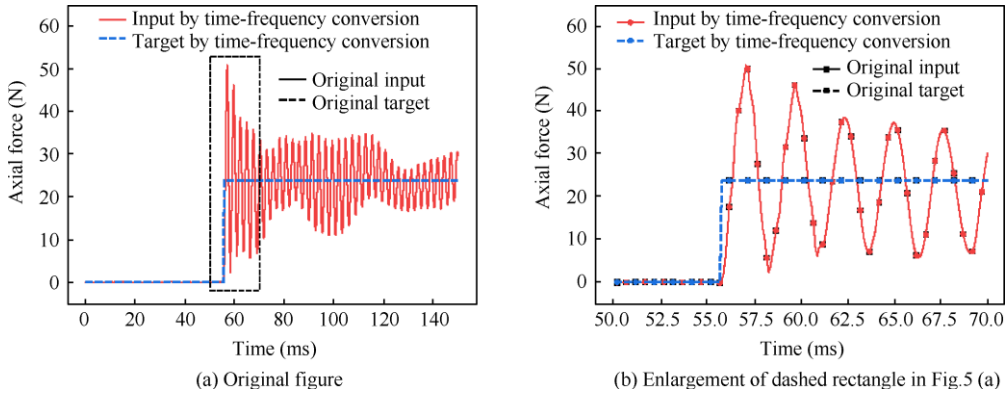

Fig 5. Verification of signal after time-frequency conversion.

3. FMS based on RNN time-domain model

3.1. Construction of RNN time-domain model

Feature extraction is a very important but difficult task for a complex artificial-intelligence problem. Deep learning approximates complex functions by stacking multilayer nonlinear mappings, automatically learns hierarchical feature representations from the original data, and uses these combined features to solve complex problems. [40, 41] Aimed at the vibration interference signal in the balance signal samples, the neural-network model is built based on supervised learning in deep learning; the intelligent model can automatically extract the basic features of the vibration interference signal and combine them into more-complex features so as to identify the vibration interference signal.

As a common type of neural network in deep learning, RNNs are used mainly to solve time-series problems and predict sequential data. The RNN model has the function of "memory" and the nodes

between each two layers are connected. [42, 43] As shown in Fig 6, the input of the hidden layer comprises the output of the input layer and the hidden layer at the previous moment. Because of the existence of a retarder, the recurrent hidden layer completes the storage and dependence by providing a path for information trans-mission. Therefore, an RNN can process time-sequence data effectively.

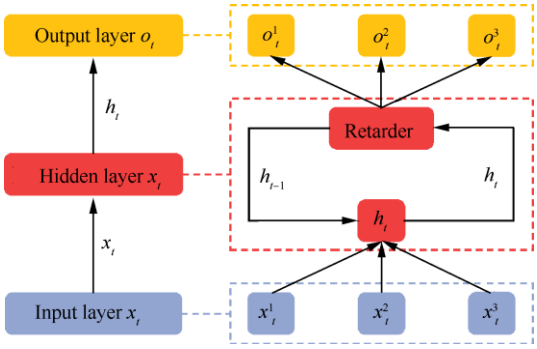

Fig 6. Unit of a Recurrent Neural Network (RNN).

To ensure consistent training samples and shock-tunnel force measurement data (test samples), the balance output signal is normalized before model training, and the data are mapped to a small specific interval. When normalizing the data, the balance output signal value is mapped to [−1,1] using the linear function:

$$x^* = \frac{x}{\max\left(|x|\right)} \tag{3}$$

where x corresponds to the original data, $\max\left(|x|\right)$ is the largest absolute value in the original data, and x^* corresponds to the normalized data. After the training, the inverse-normalization function

$$x = \max\left(|x|\right)x^* \tag{4}$$

is used to restore the data to the original interval.

The number of the training samples is 120 and the number of the points per training sample is 7500. The output channels of the three-component balance are the normal force, the pitching moment, and the axial force. Therefore, the shapes of the input and output layer of the RNN time-domain model are $(120, 7500, 3)$. After comparing the results of different hidden layers, we confirm that the number of the hidden layers is 3 and the layer parameters are shown in Table 1.

Table 1. Layer parameters of RNN time-domain model.

Layer	Type	Output shape
Input_1	Input	(120, 7500, 3)
Bi-LSTM_2	Bidirectional LSTM	(120, 7500, 128)
Bi-LSTM_3	Bidirectional LSTM	(120, 7500, 128)
Bi-LSTM_4	Bidirectional LSTM	(120, 7500, 128)
Output_5	Output	(120, 7500, 3)

3.2. Validation and error analysis of RNN time-domain model results

As shown in Fig 7, we select a representative validation sample and compare it with its output data processed by the RNN time-domain model of axial force; the red and black lines represent the input and target data, respectively, and the blue line represents the output signal processed by the RNN time-domain model. Fig 7 shows that most of the vibration signals in the input data have been eliminated; the blue line almost coincides with the black line, meaning that the output signal meets the requirements of the ideal step signal. The value of the processed data is approximately 0 before the signal step and remains constant thereafter, so the signal processed by the RNN time-domain model

achieves a steady state and most of the vibration interference signals are eliminated.

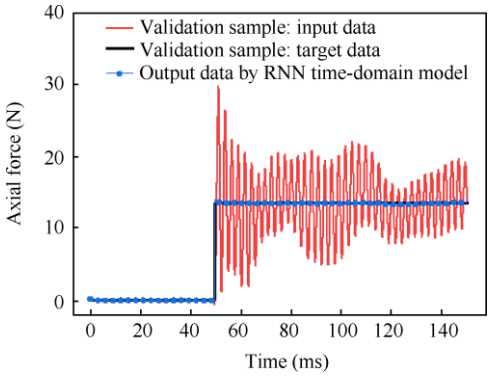

Fig 7. Validation of axial force processed by RNN time-domain model.

The normal force and pitching moment are processed in the same way, and their comparison results are shown in Fig 8. As can be seen, the processed results of the RNN time-domain model are relatively good and achieve the expected effect.

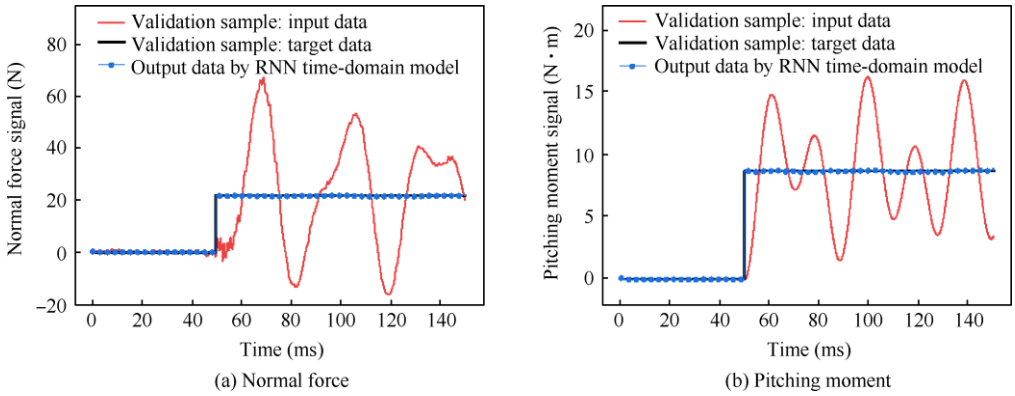

Fig 8. Validation of processing by RNN time-domain model.

Herein, we use the Mean Squared Error (MSE) as a loss function to evaluate the data processing capability of the intelligent models: the smaller the MSE, the better the quality of the predicted test data. Fig 9 shows how the loss of the RNN time-domain model changes with the training time (epoch), where the red and blue lines represent the training and validation losses, respectively, in the model training process. The model loss is approximately 10^{-2} initially, and with more epochs it decreases gradually and becomes steady. After 20000 epochs, the model validation loss has decreased to 3×10^{-5}, which is deemed sufficiently small and basically steady. This indicates that the model has converged and reached the standard for effective dynamic calibration, thereby verifying the feasibility of the data processing method of the RNN time-domain model.

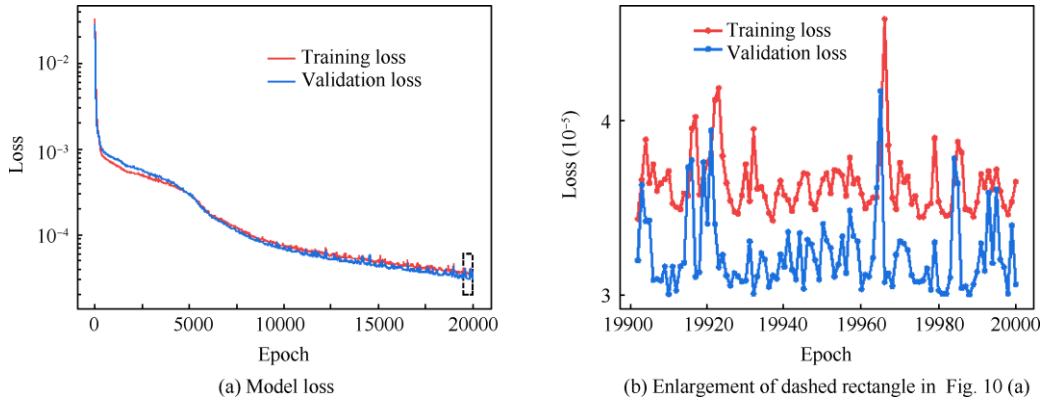

Fig 9. Loss of the RNN time-domain model decreases with number of epoch.

To evaluate more intuitively the quality of the data processed by the RNN time-domain model, we use

the relative error and the relative standard deviation RSD to evaluate the accuracy and precision of the model. These are calculated as

$$\delta = \frac{\bar{F}^* - \bar{F}}{\bar{F}} \times 100\% \tag{5}$$

$$\mathrm{RSD} = \frac{1}{\bar{F}^*}\sqrt{\frac{1}{N-1}\sum_{i=1}^{N}\left(F_i^* - \bar{F}^*\right)^2} \times 100\% \tag{6}$$

We analyze the step signals in Fig 7 and Fig 8, i.e., the data in the interval of 60 – 140 ms. Here, $\bar{F}$ is the mean value of the ideal step signal (used to represent the "true" force) and $\bar{F}^*$ is the mean value of the results processed by the RNN time-domain model (used to represent the approximate force).

The calculation results are given in Table 2. As can be seen, the relative errors of the RNN time-domain model are relatively small, especially that for the axial force, which is less than 0.1%, indicating that the accuracy of the model is relatively high. Meanwhile, the relative standard deviations of the three components are also relatively small, being basically less than 1%, indicating the high precision of the model. The model achieves high accuracy in the overall data processing, with that of the axial force being obviously better than those of the normal force and pitching moment. One reason for this is that while acquiring balance samples, the inertial vibration characteristic of the axial force component is more obvious and its signal periodicity is stronger, whereas the other two components suffer greatly from environmental noise; another reason is that the accuracy of static calibration for the axial force is better than those for the normal force and pitching moment. Therefore, the subsequent analysis is focused on the axial force and not the other two components.

Table 2. Relative error and relative standard deviation of RNN time-domain model.

Component	$\bar{F}$	$\bar{F}^*$	δ **(%)**	**RSD (%)**
Normal force	21.955 N	21.632 N	−1.47	0.582
Pitching moment	8.694 N·m	8.674 N·m	−0.229	0.561
Axial force	13.489 N	13.482 N	−0.0506	0.433

4. FMS based on CNN frequency-domain model

4.1. Construction and optimization of CNN frequency-domain model

When a force measurement is conducted in a shock tunnel, the balance output signal is rather complex, containing the aerodynamic force, inertial vibration, and other interference signals. The aerodynamic force and inertial vibration of the FMS differ greatly in the frequency domain: the aerodynamic signal is affected by the shock-tunnel flow field and other factors, so its frequency varies with time, whereas the inertial vibration frequency is an inherent attribute of the system; when the mass and structure of the FMS are determined, the inertial vibration frequency is also determined and remains stable within the test duration. Therefore, the frequency-domain signal reflects the inertial vibration characteristics of the FMS more accurately in essence.

As a classic neural network in deep learning, CNN models have been used widely in image recognition, sentence classification, data fitting, and other intelligent fields. [44] The recognition of the inertial vibration feature of the FMS in the frequency domain tends to be an image recognition problem, so we use a CNN to build a frequency-domain model for recognizing the inertial vibration feature. Fig 10 shows a flowchart of the CNN frequency-domain model. The input and output layer comprise the balance signal samples processed by FFT and the expected results processed by the model, respectively. The shapes of the input and output layer of the model are $(120,2,7500,3)$. The hidden layers comprise several convolutional and pooling layers. In deep learning, the quality of a CNN model is improved mainly by adjusting the number of convolutional layers and the number of epochs.

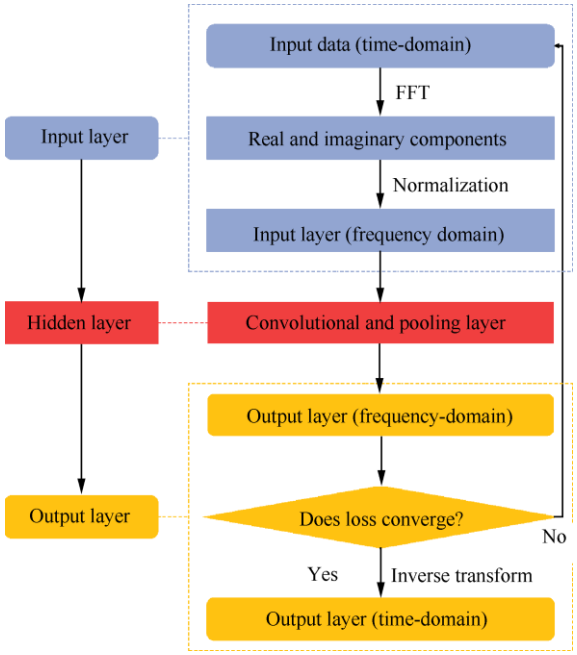

Fig 10. Flowchart of a Convolutional Neural Network (CNN) frequency-domain model.

The number of convolutional layers can directly affect the training time and accuracy of the model. Increasing the number of convolutional layers can reduce the number of parameters when the model achieves the same expressiveness. Keeping the other parameters the same, we calculate the relative error and relative standard deviation with different numbers of convolutional layers based on Eqs. (5) and (6). The comparison results when the number of convolutional layers is 24, 64 and 96 are shown in Table 3.

Table 3. Comparison with different numbers of convolutional layers of the CNN frequency-domain model.

Convolutional layer number	$\bar{F}$ (N)	$\bar{F}^*$ (N)	δ (%)	RSD (%)
24	12.745	12.735	−0.08	0.94
64	12.745	12.530	−1.69	0.39
96	12.745	12.475	−2.12	0.29

According to Table 3, when the number of convolutional layers increases from 24 to 96, it can be found that the relative error increases gradually, while the relative standard deviation decreases obviously, and the training time increases obviously. Therefore, considering them comprehensively, the number of convolutional layers is determined to be 64.

After determining the number of convolutional layers, the number of epochs is optimized. Increasing the number of epochs can improve the accuracy of the model, but the training time will increase significantly. The relative error and relative standard deviation with different numbers of epochs are shown in Table 4.

Table 4. Comparison with different numbers of epochs of CNN frequency-domain model.

Epoch number	$\bar{F}$ (N)	$\bar{F}^*$ (N)	δ (%)	RSD (%)
10000	12.745	12.720	−0.20	2.19
50000	12.745	12.580	−1.29	1.00
100000	12.745	12.530	−1.69	0.39

Table 4 shows the results processed by the CNN frequency-domain model when the number of epochs is 10000, 50000 and 100000 respectively. It can be seen that when the number of epochs increases,

the relative error increases, and the relative standard deviation decreases. Therefore, we choose the number of epochs as 100000.

After the above comparison, the parameters of the CNN frequency-domain model are optimized, and the finally number of convolutional layers and epochs are 64 and 100000, respectively.

4.2. Validation and error analysis of results from CNN frequency-domain model

The optimized CNN frequency-domain model is used to process the dynamic samples. To analyze the model quality more intuitively, the output signal processed by the model is compared with the ideal step signal in the frequency and time domains as shown in Fig 11, where the blue line represents the output signal processed by the model. As can be seen, in the frequency domain, the inertial vibration interference of 380 Hz in the input data is eliminated completely, and in the time domain, the output signal obviously meets the requirement of the ideal step signal.

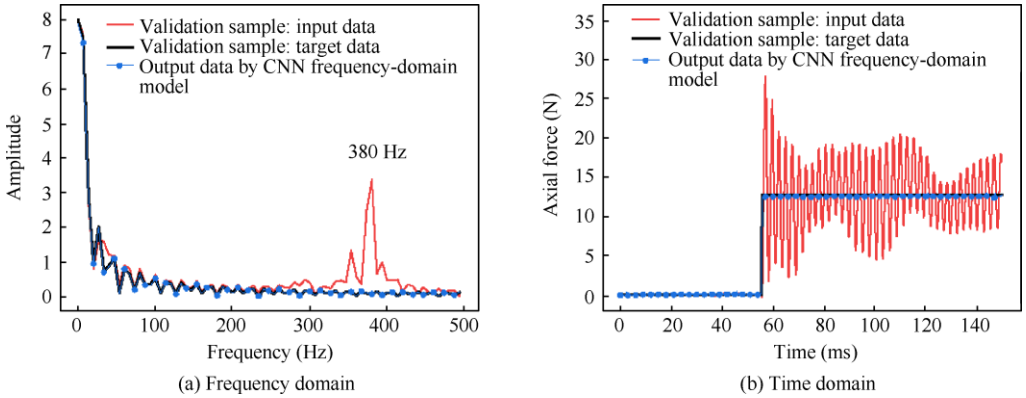

Fig 11. Validation of axial force processed by CNN frequency-domain model.

Similar to those with the RNN time-domain model, we calculate the relative error and relative standard deviation of the CNN frequency-domain model, as given in Table 5. The mean of the output data processed by the model is close to that of the ideal step signal, and its relative error is approximately 2%, which verifies that the accuracy is high and the model is reliable. Also, the relative standard deviation is only 0.39%, indicating that the output data are very steady during this period. Therefore, the CNN frequency-domain model has high accuracy and precision and is very reliable for data processing.

Table 5. Relative error and relative standard deviation of CNN frequency-domain model.

Component	$\bar{F}$ (N)	$\bar{F}^*$ (N)	δ (%)	RSD (%)
Axial force	12.745	12.530	−1.69	0.39

5. Application of intelligent model methods of force measurements from JF-12 shock tunnel

The validation and analysis of the RNN time-domain and CNN frequency-domain models show that they dealt very well with the inertial vibration interference signals in the training samples, so now we apply these two intelligent models to dynamic calibration of the FMS in a shock tunnel. In order to verify the reliability of the modeling method, a force measurement experiment was carried out in JF-12 shock tunnel. The experimental model is a standard cone, with a half-cone angle of and a length of 0.75 m (HSCM-2). [45] Fig 12 shows the force measurement experiment in JF-12 shock tunnel.

Fig 12. Validation of axial force processed by CNN frequency-domain model. Force test in JF-12 shock tunnel.

After the force measurement experiment, the output signals of balance were reprocessed by the RNN time-domain and CNN frequency-domain models, and the results are shown in Fig 13. As can be seen, the inertial vibration of 380 Hz is eliminated in the frequency domain, and the output signal processed by the models is mostly free of vibration interference. Compared with the time waveform processed by the RNN time-domain model, that processed by the CNN frequency-domain model is steadier. The results for the validation sample in Fig 11 are better than those for the test sample in Fig 13, the main reason being that the test signal is more complex and the real aerodynamic signal is not absolutely steady; there is still a certain amount of deviation between the processed signal and the ideal step signal.

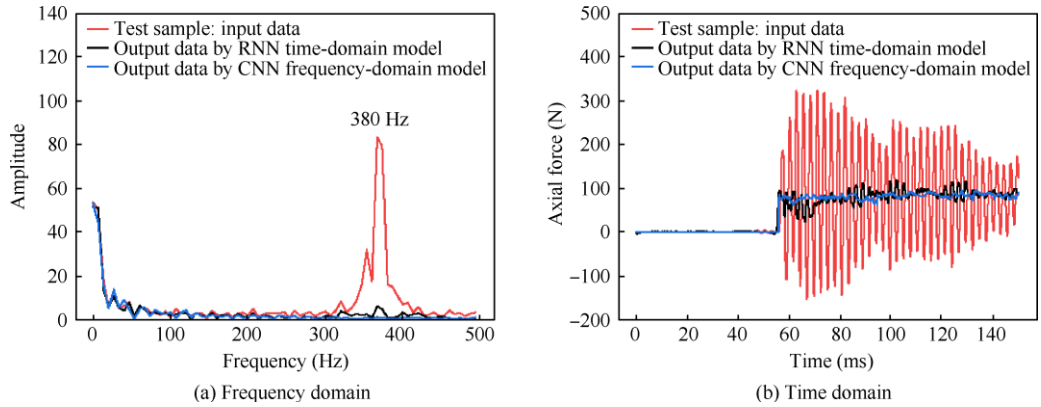

Fig 13. Comparison of axial force processed by RNN time-domain and CNN frequency-domain models.

Similar to the data processing method for the training samples, we calculate the relative deviation RD and the relative standard deviation for the RNN time-domain and CNN frequency-domain models. The results in Table 6 show that after the force measurement signal is processed by these two intelligent models. When compared with results from the force measurement database for the cone model, the relative deviation is less than 2 %, validating the feasibility of applying deep learning methods in pulse-type shock tunnel balance force tests. The current method has high accuracy in processing the shock-tunnel balance signal and can recognize the inertial vibration features of the FMS effectively. Deep-learning modeling based on an RNN in the time domain and a CNN in the frequency domain has high application value in processing dynamic force measurement signals from shock tunnels, and we will continue to carry out more in-depth research on the cross-application of deep-learning technology in dynamic signal analysis. The next step in model training will be to increase the numerical number of

samples. Meanwhile, in the process of sample acquisition, the environmental noise can be eliminated properly to ensure consistency between training and test samples to improve the model quality.

Table 6. Comparison of RNN time-domain and CNN frequency-domain models (axial component).

Model	$\bar{A}$	$\bar{A}^*$	RD (%)	RSD(%)
RNN	0.1026	0.1031	0.49	16.49
CNN	0.1026	0.1012	−1.36	6.56

6. Conclusions

(1) According to different characteristics of the balance signal in the time domain and the frequency domain, the corresponding intelligent models were proposed. An intelligent RNN model in the time domain and an intelligent CNN model in the frequency domain were trained to process the balance signal, and the results show that the two intelligent models recognized the inertial vibration characteristics of the FMS effectively.

(2) The aerodynamic signals processed by the models were steady. When compared with results from the force measurement database for the cone model, the relative deviation is less than 2 %, validating the feasibility of applying deep learning methods in pulse-type shock tunnel balance force tests.

(3) The proposed modeling method is universal in force tests in shock tunnel. The RNN model and CNN model can be used to process the complex characteristics in the time domain and the frequency domain, respectively. The present modeling method based on deep learning is feasible for shock-tunnel force tests and has great engineering value. Exploring new data processing techniques with different neural-network models could provide more reliable data for research in hypersonic vehicles.

References

1. Baals DD. *Wind tunnels of NASA*. Washington, D.C.: NASA; 1981.
2. Squire LC. A review of the role of some small high-speed wind tunnels in aeronautical research. *Prog Aerosp Sci* 1998;**34**(3–4):107–66.
3. Zong Q, Zeng FL, Zhang XB, et al. *Modeling and model verification of hypersonic aircraft*. Beijing: Science Press; 2016 [Chinese].
4. He DX. *Wind tunnel balance*. Beijing: National Defense Industry Press, 2001 [Chinese].
5. Bernstein L, Pankhurst RC. Force measurements in short-duration hypersonic facilities. Pairs: Advisory Group for Aerospace Research and Development Neuilly-Sur-Seine; 1975.
6. Naumann KW, Ende H, Mathieu G. Technique for aerodynamic force measurement within milliseconds in shock tunnel. *Shock Waves* 1991;**1**(3):223–32.
7. Storkmann V, Olivier H, Gronig H. Force measurements in hypersonic impulse facilities. *AIAA J* 1998;**36**(3):342–8.
8. Sanderson SR, Simmons JM. Drag balance for hypervelocity impulse facilities. *AIAA J* 1991;**29**(12):2185–91.
9. Mee DJ, Daniel WJT, Simmons JM. Three-component force balance for flows of millisecond duration. *AIAA J* 1996;**34**(3):590–5.
10. Smith AL, Mee DJ, Daniel WJT, et al. Design, modelling and analysis of a six component force balance for hypervelocity wind tunnel testing. *Comput Struct* 2001;**79**(11):1077–88.
11. Robinson MJ, Mee DJ, Tsai CY, et al. Three-component force measurements on a large scramjet in a shock tunnel. *J Spacecr Rockets* 2004;**41**(3):416–25.
12. Robinson MJ, Schramm JM, Hannemann K. Design and implementation of an internal stress wave force balance in a shock tunnel. *CEAS Space J* 2011;**1**(1):45–57.
13. Duryea GR, Martin JF. An improved piezoelectric balance for aerodynamic force. *IEEE Trans Aerosp Electron Syst* 1968;**AES-4**(3):351–9.
14. Li SC, Li KS, Liu BK, et al. A new dynamic modelling methodology of a force measuring system for hypersonic impulse wind tunnel. *Measurement* 2020;**164**: 108012.
15. Li SC, You ZC, Gao HL, et al. Force measurement and support integrated device in hypersonic wind tunnel. *IEEE Trans Instrum Meas* 2022;**71**: 1–9.
16. Naumann KW, Ende H, Mathieu G, et al. Millisecond aerodynamic force measurement with side-jet model in theISL shock tunnel. *AIAA J* 1993;**31**(6):1068–74.

17. Laurence SJ, Butler CS, Martinez Schramm J, et al. Force and moment measurements on a free-flying capsule in a shock tunnel. *J Spacecr Rockets* 2018;**55**(2):403–14.
18. Tanno H, Komuro T, Sato K, et al. Free-flight measurement technique in the free-piston high-enthalpy shock tunnel. *Rev Sci Instrum* 2014;**85**(4):045112.
19. Mizuno T, Ishino Y, Takasaki M. Fabrication of a three-dimensional force measurement system using double series magnetic suspension. *IFAC-PapersOnLine* 2016;**49**(21):536–40.
20. Wang YP, Liu YF, Luo CT, et al. Force measurement using strain-gauge balance in a shock tunnel with long test duration. *Rev Sci Instrum* 2016;**87**(5):055108.
21. Wang Y, Liu Y, Jiang Z. Design of a pulse-type strain gauge balance for a long-test-duration hypersonic shock tunnel. *Shock Waves* 2016;**26**(6):835–44.
22. Wang Y, Jiang Z. Impulse force-measurement system. *Shock Waves* 2020;**30**(6):603–13.
23. Sahoo N, Mahapatra DR, Jagadeesh G, et al. An accelerometer balance system for measurement of aerodynamic force coefficients over blunt bodies in a hypersonic shock tunnel. *Meas Sci Technol* 2003;**14**(3):260–72.
24. Joarder R, Jagadeesh G. A new free floating accelerometer balance system for force measurements in shock tunnels. *Shock Waves* 2003;**13**(5):409–12.
25. Tanno H, Komuro T, Takahashi M, et al. Unsteady force measurement technique in shock tubes. *Rev Sci Instrum* 2004;**75**(2):532–6.
26. Saravanan S, Jagadeesh G, Reddy KPJ. Aerodynamic force measurement using 3-component accelerometer force balance system in a hypersonic shock tunnel. *Shock Waves* 2009;**18**(6):425–35.
27. Marineau EC, MacLean M, Mundy EP, et al. Force measurements in hypervelocity flows with an acceleration compensated strain gage balance. *J Spacecr Rockets* 2012;**49**(3):474–82.
28. Lv JZ, Zhang XQ, Chen GX, et al. Transient dynamics research on the force-measurement system for hypersonic impulse combustion wind tunnel based on inertia compensation. *J Aerosp Eng* 2018;**31**(6): 04018094.
29. Lv JZ, Zhang X, Chen G, et al. Transient simulation for dynamic output of force measuring balance in an impulse combustion wind tunnel based on inertia compensation. *Journal of Vibration and Shock* 2018; **37**(2): 216–22 [Chinese].
30. Luo CT, Wang YP, Wang C, et al. Wave system fitting: A new method for force measurements in shock tunnels with long test duration. *Mech Syst Signal Process* 2015;**62–63**: 296–304.
31. Luo C, Wang Y, Hu Z, et al. Weighting by cross-validation: A calibration method for force measurements via transient response analysis. *Exp Tech* 2019;**43**(4):469–78.
32. Nie SJ, Wang YP. Signal analysis and processing of shock tunnel balance based on time-frequency transform. *Chinese Journal of Theoretical and Applied Mechanics* 2022;**54**(1):232–43 [Chinese].
33. Wang YP, Yang RX, Nie SJ, et al. Deep-learning-based intelligent force measurement system using in a shock tunnel. *Chinese Journal of Theoretical and Applied Mechanics* 2020;**52**(5):1304–13 [Chinese].
34. Wang QC, Li SC, Gao HL, et al. Research on intelligent identification algorithms for short-term aerodynamics of hypersonic wind tunnels. *Chinese Journal of Theoretical and Applied Mechanics* 2022;**54**(3):688–96 [Chinese].
35. Wang YP, Hu ZM, Liu YF, et al. Starting process in a large-scale shock tunnel. *AIAA J* 2016;**54**(4):1240–9.
36. Garland PP, Rogers RJ. Dynamic calibration of tri-axial piezoelectric force transducers. *Meas Sci Technol* 2008;**19**(9):095202.
37. Li B. Characteristics' experimental study on the 6-ssr six degree-of-freedom accelerometer[dissertation]. Qinhuangdao: Yanshan University; 2011 [Chinese].
38. Yang SL. Studies on dynamic characteristics and dynamic correction methods for wind tunnel strain gauge balance[dissertation]. Hefei: Hefei University of Technology; 2014 [Chinese].
39. Wang YP, Jiang ZL. Intelligent force-measurement system used in shock tunnel. *Sensors* (*Basel*) 2020;**20**(21):6179.
40. Sun ZJ, Xue L, Xu YM, et al. Overview of deep learning. *Application Research of Computers* 2012;**29**(8):2806–10.
41. Du XD, Cai YH, Wang S, et al. Overview of deep learning. *2016 31st Youth Academic Annual Conference of Chinese Association of Automation (YAC)*; Wuhan, China. Piscataway: IEEE; 2017.p.159–64.
42. De Mulder W, Bethard S, Moens MF. A survey on the application of recurrent neural networks to statistical language modeling. *Comput Speech Lang* 2015;**30**(1):61–98.
43. Van Houdt G, Mosquera C, Nápoles G. A review on the long short-term memory model. *Artif Intell Rev* 2020;**53**(8):5929–55.
44. Yao GL, Lei T, Zhong JD. A review of Convolutional-Neural-Network-based action recognition. *Pattern Recognit Lett* 2019;**118**: 14–22.
45. General Armament Department of Chinese people's Liberation Army. *Aerodynamic test method in hypersonic wind tunnel: GJB 4399-2002*, 2002. [Standard]. [Chinese].
46. General Armament Department of Chinese people's Liberation Army. *Specification for wind tunnel strain gage balance: GJB 2244A-2011*, 2011. [Standard]. [Chinese].